Real-time dynamic substructuring in a coupled oscillator-pendulum system

By Y.N. Kyrychko[1], K.B. Blyuss[2], A. Gonzalez-Buelga[3], S.J. Hogan[1], D.J. Wagg[3]

[1]*Department of Engineering Mathematics, University of Bristol, Queen's Building, Bristol BS8 1TR, UK*

[2]*Department of Mathematical Sciences, University of Exeter, Laver Building, Exeter EX4 4QE, UK*

[3]*Department of Mechanical Engineering, University of Bristol, Queen's Building, Bristol BS8 1TR, UK*

Real-time dynamic substructuring is a powerful testing method which brings together analytical, numerical and experimental tools for the study of complex structures. It consists of replacing one part of the structure with a numerical model, which is connected to the remainder of the physical structure (the substructure) by a transfer system. In order to provide reliable results, this hybrid system has to remain stable during the whole test. One of the problems with the method is the presence of delay (due to several technical factors) which can lead to destabilization and failure. In this paper we apply the dynamic substructuring technique to a simple nonlinear system, consisting of a pendulum attached to a mass-spring-damper. The latter is replaced by a numerical model and the transfer system is an actuator. The system dynamics is governed by two coupled second order neutral delay differential equations. We carry out a stability analysis of the system and identify possible regions of instability and the number of stability switches depending on parameters and the size of the delay. Using the parameters from a real experiment, we perform numerical simulations which confirm our analytical findings, and show regions of periodic and quasi-periodic behaviour. We also confirm our stability results by comparison with an experiment. The agreement is excellent.

Keywords: stability analysis; real-time testing; neutral delay equation; hopf bifurcation; numerical simulations

1. Introduction

There are several methods for predicting the dynamic response of structures to external forces. These can be analytical methods, which work well if the structure is simple and linear, and numerical methods which are usually used for nonlinear structures. In both cases, the approach is one where a mathematical model is used to approximate the behaviour of a physical system. For complex systems, mathematical models may contain significant uncertainty and it is often better to build prototype models and to perform tests in the laboratory. In case when the complex system is very large (such as a cable-stayed bridge or an airplane) such an approach may be impractical, very expensive or both. In these cases there is a need to develop a formalism which can include the benefits of both theoretical and

experimental methods whilst at the same time avoiding their drawbacks. Such a hybrid testing method could help to reduce the overall cost of the experiment and at the same time offer the possibility of observing full scale dynamics.

One such approach is real-time dynamic substructuring (see, for instance, Blakeborough *et al.* 2001; Bonelli & Bursi 2004; Horiuchi & Konno 2001; Nakashima 2001; Pinto *et al.* 2004; Wallace *et al* 2004; Williams & Blakeborough 2001). This method consists of dividing the test structure into two parts. One part is modelled numerically and the other is a physical substructure which is placed in the laboratory. The two parts are linked through a transfer system, usually sets of actuators. A significant concern is to ensure that the substructure and its numerical counterpart behave in the same way as the full structure. One of the main obstacles with this approach is the presence of delay.

Delay arises because of the non-instantaneous nature of the transfer system. In fact, there can be a number of different delays from several different sources, such as data acquisition, computation, digital signal processing and the actuator itself, which all contribute to produce an overall delay. In general, the dynamics of the transfer system (depending on its configuration) should be described by an inclusion of time delay and a frequency dependent delay (or time lag). However, the experiment presented in this paper has a transfer system represented by an electro-dynamic actuator, and we are working in the regime of small frequencies. This means that in this case the dependence of time delay on frequency of external excitation is negligible, and therefore, we treat time lag as a fixed time delay. This convention has been successfully used by several authors, including Darby *et al.* (2001) and Darby *et al.* (2002). We have also produced the transfer system response plots 2 (a)), with the transfer function written via Laplace transform as $Y(s) = \dfrac{56.02}{s + 55.55}$, and experimental frequency sweep testing is presented in Figure 2 (b)). Therefore the dynamics of the numerical part will be modelled using delay differential equations, or DDEs (partial or ordinary, depending on the complexity of the system). These equations depend not only on the current state of the system, but also on the history of the system over some previous time interval (the delay). Hence, the initial state space and the solution space of the delayed dynamical system are infinite dimensional. The theory of this type of equations lies in the area of functional differential equations discussed in details by Wu (1996), and some methods and results with applications to engineering problems can be found in Xu & Chung (2003).

In this paper we concentrate on an example of a system to which the hybrid testing technique can be applied. The system consists of a pendulum coupled to a mass-spring damper (MSD). The MSD is taken to be the numerical model and the pendulum, the physical substructure, was constructed in the laboratory. The pendulum is attached to the side of the rig by means of a pivot. This allows the pendulum to swing in the xy-plane. The transfer system is an electrically driven ball-screw actuator. The full system and its hybrid equivalent are depicted in figure 1. The implementation of the real-time experiment was done by using a dSpace DS1104 RD Controller Board. The detailed description of the experiment as well as experimental results can be found in Gonzalez-Buelga *et al.* (2005). The particular reason for choosing this example lies in the fact that there is a straightforward way to divide the structure into linear and non-linear parts. The possible applications of

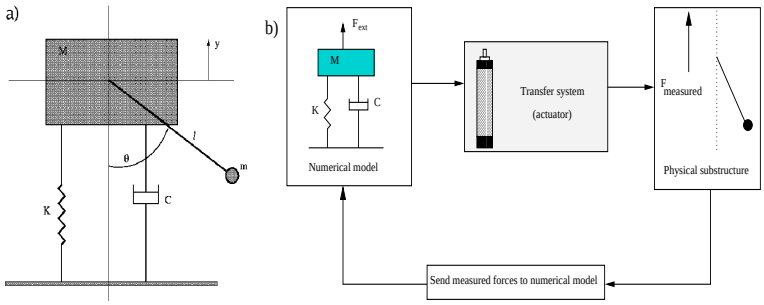

Figure 1. (a) Full coupled pendulum-MSD system. (b) Real-time dynamic substructuring system showing numerical model, transfer system and physical substructure.

coupled pendulum-MSD systems include the modelling of human leg motion (see, for example, Coveney *et al.* 2001; Lafortune & Lake 1995).

In order to investigate whether the hybrid system of substructure and numerical model (figure 1(a)) behaves in the same way as the full structure would behave (figure 1(b)), we propose a model represented by delay differential equations. The whole system should remain stable during a test. However, delays can destabilize the system, giving rise to oscillatory, periodic or even chaotic solutions not present in the original non-delayed system. Therefore, a full mathematical analysis and numerical simulations based on experimental values of parameters will provide detailed information about the influence of delay on stability of the system. This will help to determine and then implement a delay compensation technique to be used in the experiment. The approach of using delay differential equations for mathematical modelling of hybrid testing has been first proposed by Wallace *et al.* (2004) and Wallace *et al.* (2005). The authors considered a simple mass-spring oscillator and demonstrated the dependence of stability of the system on delay. Significant difference of the present work from earlier studies is the fact that we consider a nonlinear and neutral system of delay differential equations. For the general references on the theory of DDEs see, for example, Kuang (1993), Diekmann *et al.* (1995), Stépan (1989) and references therein.

The paper is organized as follows: in Section 2 we introduce a system of delay differential equations describing the coupled pendulum-MSD system. Section 3 is devoted to the stability analysis of the neutral DDE. In Section 4 stability of periodic solutions is investigated by means of multiple scale analysis for the case of near resonant soft excitation. Section 5 contains numerical simulations which confirm our analytical findings. The linearized stability analysis of the coupled non-linear system of delay differential equations is presented in Section 6. Section 7 contains a comparison between experimental and analytical results. In Section 8 the effects of viscous damping are studied. The paper concludes with a summary of results in Section 9.

2. The equations of motion

Consider a mechanical system which consists of a mass M mounted on a linear spring, to which a pendulum of mass m is attached via a hinged massless rod of length ℓ. The angular deflection of the pendulum from the downward position is

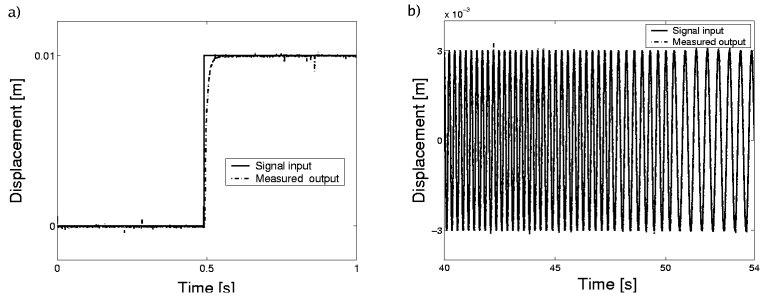

Figure 2. (a) Transfer function step response. (b) Frequency sweep plot.

denoted by θ. We assume linear viscous damping C acting on the mass M. The system is shown schematically in figure 1. The equations of motion for our system are

$$\begin{aligned} M\ddot{y}(t) + C\dot{y}(t) + Ky(t) &= F_{\text{ext}} - m\ddot{y} - m\ell[\ddot{\theta}\sin\theta + \dot{\theta}^2\cos\theta], \\ m\ell^2\ddot{\theta}(t) + \kappa\dot{\theta}(t) + mg\ell\sin\theta(t) + m\ell\ddot{y}\sin\theta(t) &= 0, \end{aligned} \tag{2.1}$$

where

$$F_{\text{ext}} = k\cos(\Omega t),$$

is the external excitation force applied in the y direction, C and K are the damping and stiffness coefficients respectively, and a dot indicates the derivative with respect to time t. We will refer to $y(t)$, $\dot{y}(t)$ and $\ddot{y}(t)$ as the position, velocity and acceleration of the MSD at time t. There are three important frequencies associated with this system: the natural frequency of the pendulum ω_0, where $\omega_0^2 = g/\ell$, the natural frequency of the mass-spring-damper ω_1, where $\omega_1^2 = K/(M+m)$ and the frequency Ω of the external excitation force. The situation where the natural frequencies of the MSD and the pendulum are in $2:1$ resonance has been widely studied in the literature (see Tondl *et al.* 2000 and references therein).

Since the transfer system produces an unavoidable delay in the system, the feedback force will be delayed. The time delay is denoted by τ and it is assumed to be constant and non-negative. To account for the delay in the displacement signal, the force in the system (2.1) has to be described by the delayed state of the numerical model of the MSD. Therefore, in the RHS of the first equation in (2.1) we replace $y(t)$ and $\theta(t)$ by their delayed counterparts: $y(t-\tau)$ and $\theta(t-\tau)$ respectively. The same has to be done for *all* terms in the second equation of the system (2.1). By inserting these expressions in system (2.1), we obtain the following

$$\begin{aligned} &M\ddot{y}(t) + C\dot{y}(t) + Ky(t) + m\ddot{y}(t-\tau) \\ &+m\ell[\ddot{\theta}(t-\tau)\sin\theta(t-\tau) + \dot{\theta}^2(t-\tau)\cos\theta(t-\tau)] = k\cos(\Omega t), \\ &m\ell^2\ddot{\theta}(t-\tau) + \kappa\dot{\theta}(t-\tau) + mg\ell\sin\theta(t-\tau) + m\ell\ddot{y}(t-\tau)\sin\theta(t-\tau) = 0. \end{aligned} \tag{2.2}$$

The main goal of this paper is to analyse (2.2), the equations of the hybrid system, to see under what circumstances they produce the same dynamics as those of (2.1) and to confirm these results by experiment. In particular we will be looking at the stability of the so-called trivial solution in which the MSD moves (so $y(t) \neq 0$ in general) but the pendulum does not oscillate (so $\theta(t) = 0$ in general).

3. Stability analysis of the neutral delay differential equation

First, we consider the case when the angle θ is small ($\theta \ll 1$). In this case the system (2.2) decouples and we concentrate on the first equation, which describes the vertical motion of the pendulum-MSD system. In the absence of external forcing ($k = 0$), linearization of this equation around the trivial solution leads to the equation

$$M\ddot{y}(t) + C\dot{y}(t) + Ky(t) + m\ddot{y}(t-\tau) = 0. \tag{3.1}$$

Since the delayed system depends on the acceleration of the state variable, equation (3.1) is of a neutral type. We introduce the following non-dimensional variables:

$$\hat{t} = \omega_2 t,\ \hat{\tau} = \omega_2 \tau,\ \omega_2 = \sqrt{\frac{K}{M}},\ p = \frac{m}{M},\ \zeta = \frac{C}{2\sqrt{MK}}.$$

Under this rescaling and dropping the hats, equation (3.1) becomes

$$\ddot{z} + 2\zeta\dot{z} + z + p\ddot{z}(t-\tau) = 0, \tag{3.2}$$

where dot means differentiation with respect to t. This equation has one trivial steady state $z = \dot{z} = 0$. The corresponding characteristic equation is

$$\lambda^2 + 2\zeta\lambda + 1 + p\lambda^2 e^{-\lambda\tau} = 0. \tag{3.3}$$

When $\tau = 0$, one obtains $\lambda = \left(-\zeta \pm \sqrt{\zeta^2 - 1 - p}\right)/(1+p)$, so the steady state $z = 0$ is locally asymptotically stable. In the case $|p| > 1$, this steady state is always unstable for any positive delay τ. (This already provides us with an important consideration when constructing the hybrid system, namely that for stability we must always have $M > m$.) Therefore, we assume $|p| < 1$ in all our further analysis. The purely imaginary eigenvalues occur when $\lambda = \pm \mathrm{i}\varpi$ for $\varpi \neq 0$, so from (3.3)

$$-\varpi^2 + 2\mathrm{i}\zeta\varpi + 1 - p\varpi^2 e^{-\mathrm{i}\varpi\tau} = 0.$$

Separating into the real and imaginary parts, we arrive at the following

$$\begin{aligned} -\varpi^2 + 1 - p\varpi^2\cos(\varpi\tau) &= 0, \\ 2\zeta\varpi + p\varpi^2\sin(\varpi\tau) &= 0. \end{aligned} \tag{3.4}$$

Upon squaring and adding these equations, we obtain

$$(1-p^2)\varpi^4 + (4\zeta^2 - 2)\varpi^2 + 1 = 0.$$

Solving for ϖ gives

$$\varpi_\pm^2 = \frac{1}{(1-p^2)}\left[(1-2\zeta^2) \pm \sqrt{(1-2\zeta^2)^2 - (1-p^2)}\right]. \tag{3.5}$$

We observe that there can be either zero, one (repeated) or two real positive roots, depending on the values of p and ζ. This relation provides us with the explicit expressions for the stability boundaries, i.e. a family of solutions for the delay time τ has the form

$$\tau = \frac{1}{\varpi_\pm}\left[\mathrm{Arctan}\,\frac{2\zeta\varpi_\pm}{{\varpi_\pm}^2 - 1} \pm \pi n\right], \tag{3.6}$$

where $n = 0, 1, 2, ...$ and Arctan corresponds to the principal value of arctan.

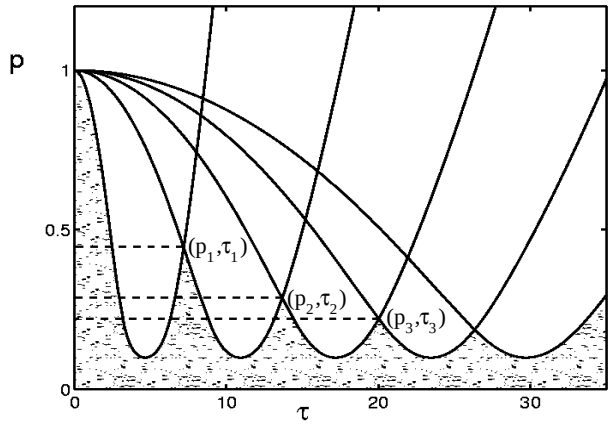

Figure 3. Stability of the trivial solution of the system (3.2) in the parameter space of delay time τ and p for $\zeta < 1/\sqrt{2}$.

Lemma 3.1. *The solution $z = \dot{z} = 0$ of the system (3.2) is locally asymptotically stable for $\zeta > \frac{1}{\sqrt{2}}$ and $|p| < 1$ independent of the delay time $\tau > 0$.*

The proof of this lemma immediately follows from the expression (3.5) for $\varpi_{\pm}$. In terms of the original parameters, the conditions of lemma 3.1 state that $C^2 > 2MK$, $M > m$. These conditions perfectly justify the choice of pendulum as the physical substructure. In the physical system, if the damping is high enough, unconditional stability is guaranteed.

Next, consider the case $\zeta < 1/\sqrt{2}$, which is depicted in figure 3. The shaded area shows the stability region. In this situation, stability of the trivial steady state strongly depends on the value of the delay τ. As τ increases from zero, the steady state undergoes a Hopf bifurcation, as a pair of complex conjugate roots of the characteristic equation crosses the imaginary axis. Under certain non-degeneracy conditions, this implies the birth of periodic solutions. We summarize our findings in the following lemma.

Lemma 3.2. *Assume $\zeta < 1/\sqrt{2}$. The trivial solution of system (3.2) is locally asymptotically stable in the region*

$$p < 2\zeta\sqrt{1-\zeta^2}, \tag{3.7}$$

for all positive delay times τ. In the region

$$2\zeta\sqrt{1-\zeta^2} \le p < 1,$$

the trivial solution is locally asymptotically stable for values of delay satisfying

$$\begin{aligned} 0 < \quad \tau \quad &< \frac{1}{\varpi_+}\left[2\pi - Arccos\,\frac{1-\varpi_+^2}{p\varpi_+^2}\right] \\ \frac{1}{\varpi_-}\left[2\pi n - Arccos\,\frac{1-\varpi_-^2}{p\varpi_-^2}\right] < \quad \tau \quad &< \frac{1}{\varpi_+}\left[(2n+2)\pi - Arccos\,\frac{1-\varpi_+^2}{p\varpi_+^2}\right], \end{aligned}$$

where $n = 1, 2, ...$

Proof. First we note that when the condition (3.7) holds, the square root

$$\sqrt{(1-2\zeta^2)^2-(1-p^2)}$$

in the definition of $\varpi_\pm^2$ (3.5) is purely imaginary. Thus the eigenvalues of the linearization matrix never cross the imaginary axis, and consequently, the trivial steady state is stable for all delay times $\tau \geq 0$ in this region.

Next, we consider the situation when $2\zeta\sqrt{1-\zeta^2} \leq p < 1$. In this case the characteristic polynomial (3.3) has two imaginary solutions $\lambda_\pm = \mathrm{i}\varpi_\pm$ with $\varpi_+ > \varpi_- > 0$ defined in (3.5). In order to determine stability as τ varies, we need to find the sign of the derivative of $\mathrm{Re}(\lambda)$ at the points where $\lambda(\tau)$ is purely imaginary. The technique we shall use has been widely applied to various characteristic equations (see, for example, Kuang 1993). Considering the function $\lambda = \lambda(\tau)$ in equation (3.3) and differentiating this equation with respect to τ, one obtains

$$\left[2\lambda + 2\zeta + p\lambda(2-\lambda\tau)e^{-\lambda\tau}\right]\frac{d\lambda}{d\tau} = p\lambda^3 e^{-\lambda\tau}.$$

From the last expression it follows that

$$\left(\frac{d\lambda}{d\tau}\right)^{-1} = 2\frac{(\lambda+\zeta)e^{-\lambda\tau}+p\lambda}{p\lambda^3} - \frac{\tau}{\lambda},$$

and from (3.3) we have

$$e^{\lambda\tau} = -\frac{p\lambda^2}{\lambda^2+2\zeta\lambda+1}.$$

Hence,

$$\mathrm{sgn}\left\{\frac{d(\mathrm{Re}\,\lambda)}{d\tau}\right\}_{\lambda=i\varpi} = \mathrm{sgn}\left\{\mathrm{Re}\left(\frac{d\lambda}{d\tau}\right)^{-1}\right\}_{\lambda=i\varpi} = \mathrm{sgn}\{2\zeta^2 - 1 + \varpi^2(1-p^2)\}.$$

Substituting $\varpi_\pm^2$ into the last expression, it is clear that the sign is positive for ϖ_+^2 and negative for ϖ_-^2. This means that as τ increases and takes a value corresponding to ϖ_+, λ crosses from the left to the right hand half of the complex plane. This implies the loss of stability of the trivial solution. Similarly, for τ corresponding to ϖ_-, the crossing is from right to left, and stability is regained. The whole process is graphically illustrated in figure 3. The proof of the lemma is complete. □

From lemma 3.2 it follows that as τ increases, the trivial equilibrium undergoes successive changes in its stability. However, it is worth noting that for fixed parameter values there is only a *finite* number of stability switches, and eventually this equilibrium becomes unstable. We can now find the number of these stability switches and the maximal delay beyond which the stability will never be recovered. The problem of constructing sequences of stability switches was addressed for first-order neutral equations by Wei and Ruan (2002).

Let us introduce a sequence

$$\{p_j : p_j > p_{j+1}, p_0 = 1, j = 1, ...\},$$

where $p_n, n = 1, ...$ solve the equation

$$\tau_-(n) = \tau_+(n+1). \tag{3.8}$$

Here we have used the notation

$$\tau_+(n) = \frac{1}{\varpi_+}\left[2\pi n - \text{Arccos}\,\frac{2\zeta\varpi_+}{{\varpi_+}^2 - 1}\right],\ \tau_-(n) = \frac{1}{\varpi_-}\left[2\pi n - \text{Arccos}\,\frac{2\zeta\varpi_-}{{\varpi_-}^2 - 1}\right].$$

Theorem 3.3. *If $p_1 \le p < 1$ there is one stability switch at $\tau_+(0)$. The trivial equilibrium is stable for $0 \le \tau \le \tau_+(0)$ and unstable for $\tau > \tau_+(0)$. If $p_{k+1} \le p < p_k$ for $k = 1, ...$, then there are exactly $(2k+1)$ stability switches, and the trivial equilibrium is stable for*

$$(0, \tau_+(0)) \cup (\tau_-(1), \tau_+(1)) \cup ... \cup (\tau_-(k), \tau_+(k)),$$

and unstable for

$$(\tau_+(0), \tau_-(1)) \cup (\tau_+(1), \tau_-(2)) \cup ... \cup (\tau_+(k), \infty).$$

For a given value of p, theorem 3.3 gives the regions of linear stability in terms of delay time τ. Unless p is smaller than the lower stability boundary $p_c = 2\zeta\sqrt{1-\zeta^2}$, there always exists a sufficiently large delay τ after which the system will be unstable. The stable boundaries of the origin can be located by the branches τ_+ and τ_- which satisfy $\tau_+(n) > \tau_-(n)$ for $n = 1, 2, ...$ For example, when τ crosses $\tau_-(1)$ the unstable origin becomes stable. When τ is increased further to cross $\tau_+(1)$, the stability is lost again as a pair of eigenvalues cross the imaginary axis into the right half plane. Similarly, other stability regions can be found for $\tau_-(n) < \tau < \tau_+(n)$. Each time we cross the stability boundary into an unstable region, the delayed action of the pendulum on the MSD leads to a destabilization of numerical model.

In the points $(p, \tau) = (p_n, \tau_n)$ the system undergoes a codimension-two Hopf bifurcation. There is a pair of complex conjugate eigenvalues crossing the imaginary axis from left to right, and there is another pair crossing from right to left. Therefore, at the above points, the system has two frequencies simultaneously present. Possible resonances in this case were studied by Campbell (1997).

4. Hopf Bifurcation

In this section the Hopf bifurcation will be investigated. Linearizing equation (2.2) with $k \neq 0$, and rescaling using $\hat{k} = k/K$ and $\hat{\Omega} = \Omega/\omega_2$, we obtain, after dropping the hats:

$$\ddot{z} + 2\zeta\dot{z} + z + p\ddot{z}(t-\tau) = k\cos\Omega t. \tag{4.1}$$

which is simply equation (3.2) with the forcing included. In order to study the criticality of the bifurcation, we will resort to a multiple scales method. Taking a delay time $\tau = \tau_c + \varepsilon\tau_1$, where τ_c is the critical delay time, we let $T = \varepsilon t$ be the new time scale and rescale equation (4.1) with $z \to \sqrt{\varepsilon}z$, $k \to \varepsilon^{3/2}k$. Physically this implies that the excitation is soft and a resonant case will be considered. In particular, we set $\Omega = \varpi_\pm + \varepsilon\sigma$, where $\sigma = \mathcal{O}(1)$ is a detuning parameter. Before

embarking on series expansion analysis, it is worth noting that since we are crossing the stability boundary, the following relation holds:

$$p = \frac{1}{\varpi_\pm^2}\sqrt{(\varpi_\pm^2 - 1)^2 + 4\zeta^2\varpi_\pm^2}.$$

Looking for solutions of equation (4.1) in the form

$$z(t) = z_0(t,T) + \varepsilon z_1(t,T) + \dots,$$

we obtain at order $\mathcal{O}(1)$

$$\frac{\partial^2}{\partial t^2}z_0 + 2\zeta\frac{\partial}{\partial t}z_0 + z_0 + p_\Omega\frac{\partial^2}{\partial t^2}z_0(t-\tau_c,T) = 0,$$

where $p_\Omega = \sqrt{(\Omega^2-1)^2 + 4\zeta^2\Omega^2}/\Omega^2$. The solution of this equation is

$$z_0(t,T) = A(T)e^{\mathrm{i}\Omega t} + A^*(T)e^{-\mathrm{i}\Omega t}, \tag{4.2}$$

where $A(T)$ is an as yet undetermined amplitude of oscillation. At order $\mathcal{O}(\varepsilon^1)$ we have

$$\frac{\partial^2}{\partial t^2}z_1 + 2\zeta\frac{\partial}{\partial t}z_1 + z_1 + p_\Omega\frac{\partial^2}{\partial t^2}z_1(t-\tau_c,T) = -2\frac{\partial}{\partial t}\frac{\partial}{\partial T}z_0 - 2\zeta\frac{\partial}{\partial T}z_0 - 2p_\Omega\frac{\partial}{\partial t}\frac{\partial}{\partial T}z_0(t-\tau_c,T)$$
$$-p_\Omega\tau_1\frac{\partial^3}{\partial t^3}z_0(t-\tau_c,T) + \sigma\hat{p}_\Omega\frac{\partial^2}{\partial t^2}z_0(t-\tau_c,T) + k\cos\Omega t, \tag{4.3}$$

with $\hat{p}_\Omega = 2(\Omega^2 - 1 - 4\zeta^2)/(\Omega^3\sqrt{(\Omega^2-1)^2+4\zeta^2})$. Substituting z_0 from (4.2) in the last expression and using complex notation, gives

$$\frac{\partial^2}{\partial t^2}z_1 + 2\zeta\frac{\partial}{\partial t}z_1 + z_1 + p_\Omega\frac{\partial^2}{\partial t^2}z_1(t-\tau_c,T)$$
$$= \left[-2\mathrm{i}\Omega A_T - 2\zeta A_T - 2\mathrm{i}p_\Omega\Omega e^{-\mathrm{i}\Omega\tau_c}A_T + \mathrm{i}\tau_1 p_\Omega\Omega^3 A - \sigma\hat{p}_\Omega\Omega^2 A + \frac{k}{2}\right]e^{\mathrm{i}\Omega t} + \text{c.c.},$$

where $A_T = \partial A/\partial T$ and *c.c.* denotes the complex conjugate. To avoid secular terms we set the bracket on the right hand side equal to zero. This gives us an equation for the amplitude A in the form:

$$-2A_T(\mathrm{i}\Omega + \zeta + \mathrm{i}p_\Omega\Omega e^{-\mathrm{i}\Omega\tau_c}) = (\sigma\hat{p}_\Omega - \mathrm{i}p_\Omega\tau_1\Omega)\Omega^2 A - \frac{k}{2}. \tag{4.4}$$

This equation can be transformed into

$$A_T = \frac{1}{2}\left[\frac{\tau_1 p_\Omega\Omega^2 + \sigma\hat{p}_\Omega\Omega^2\zeta}{\zeta^2 + 1/\Omega^2} + \mathrm{i}\frac{\sigma\hat{p}_\Omega\Omega - p_\Omega\tau_1\zeta\Omega^3}{\zeta^2 + 1/\Omega^2}\right]A - \frac{k}{4}\frac{\zeta + \mathrm{i}/\Omega}{\zeta^2 + 1/\Omega^2}.$$

Writing $A = u + \mathrm{i}v$ and separating real and imaginary parts, we obtain the following linear system of differential equations:

$$\begin{aligned} u_T &= \alpha u - \beta v + c_1, \\ v_T &= \beta u + \alpha v + c_2, \end{aligned} \tag{4.5}$$

where we have introduced the notation

$$\alpha = \frac{1}{2}\Omega^2 \frac{\tau_1 p_\Omega + \sigma \hat{p}_\Omega \zeta}{\zeta^2 + 1/\Omega^2},\ \beta = \frac{1}{2}\Omega \frac{\sigma \hat{p}_\Omega - p_\Omega \tau_1 \zeta \Omega^2}{\zeta^2 + 1/\Omega^2},$$

$$c_1 = -\frac{k}{4}\frac{\zeta}{\zeta^2 + 1/\Omega^2},\ c_2 = -\frac{k}{4}\frac{1}{\Omega(\zeta^2 + 1/\Omega^2)}.$$

System (4.5) can be solved to yield

$$\begin{aligned} u(T) &= \frac{1}{2}\frac{\sigma \hat{p}_\Omega k}{\Omega^2\left(\sigma^2 \hat{p}_\Omega^2 + p_\Omega^2 \Omega^2 \tau_1^2\right)} + C_1 e^{\alpha T}\cos\beta T + C_2 e^{\alpha T}\sin\beta T, \\ v(T) &= \frac{1}{2}\frac{p_\Omega k \tau_1}{\Omega\left(\sigma^2 \hat{p}_\Omega^2 + p_\Omega^2 \Omega^2 \tau_1^2\right)} - C_2 e^{\alpha T}\cos\beta T + C_1 e^{\alpha T}\sin\beta T. \end{aligned} \tag{4.6}$$

Thus, one can observe that the amplitude A_T of the bifurcating periodic solution is proportional to the amplitude k of the forcing, and is also modulated on a longer time scale as shown by the above expressions. If $k = 0$ (and consequently $\sigma = 0$), then depending on the sign of τ_1, the $u(T)$ and $v(T)$ exponentially tend to either 0 or $\pm\infty$, thus indicating that the periodic solution is unstable. However, if $k \neq 0$, then there is a periodic solution

$$z(t) = \frac{\sigma \hat{p}_\Omega k}{\Omega^2\left(\sigma^2 \hat{p}_\Omega^2 + p_\Omega^2 \Omega^2 \tau_1^2\right)}\cos(\Omega t + \theta_0) + \mathcal{O}(\epsilon),$$

which is stable if

$$\tau_1 p_\Omega + \sigma \hat{p}_\Omega \zeta < 0, \tag{4.7}$$

and unstable otherwise.

5. Numerical simulations

In this section we perform a numerical simulation of the system (4.1). The equation was discretized using an explicit finite difference scheme. The damping term was approximated by central differences to improve numerical stability.

For all simulations we set $p = 0.2$. In terms of the original parameters of the system this means that the mass of the pendulum is five times smaller than the mass of the MSD. At the same time, the scaled damping coefficient ζ is taken to be $\zeta = 0.05$. It readily follows that $p > 2\zeta\sqrt{1-\zeta^2}$, and one can expect a succession of stability switches for increasing values of τ.

The numerical timestep for the simulations is kept at $\Delta t = 0.01$. To illustrate the behaviour of solutions in stable and unstable regions, as discussed in section 3, we will move along the τ-axis and observe changes which occur as the stability boundaries are crossed.

We begin our numerical analysis by considering first the case when there is no external force, i.e. $k = 0$ in equation (4.1). In this situation, results from Section 3 indicate that the trivial steady state undergoes stability switches. Figure 4 shows temporal dynamics of the non-dimensionalized displacement $z(t)$ governed by equation (3.2) for several values of time delay τ. As τ is increased from zero ($\tau = 1$), the

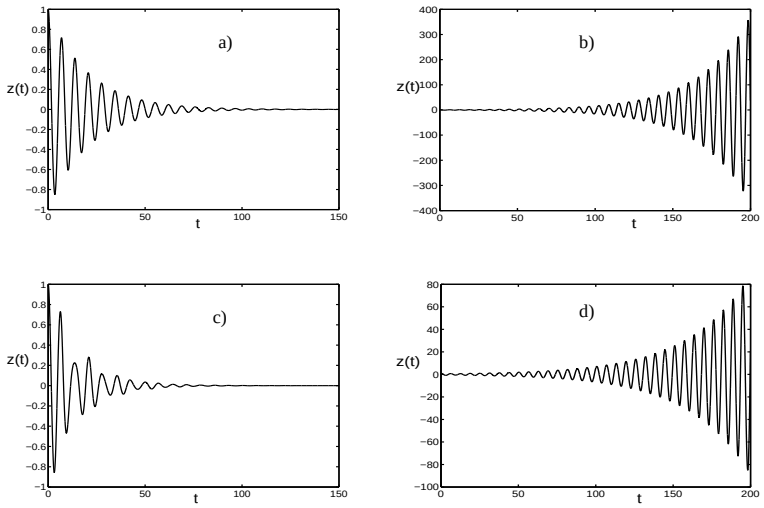

Figure 4. Temporal dynamics of $z(t)$ of system (3.2) for (a) $\tau = 1$, (b) $\tau = 5$, (c) $\tau = 7.5$ and (d) $\tau = 11$.

solution remains asymptotically stable and quickly decays to the trivial steady state (figure 4(a)). Since oscillatory decay is observed, this indicates that the eigenvalues of characteristic equation have non-zero imaginary part. Figure 4(b) shows the situation when the first switch from stability to instability has occurred ($\tau = 5$). The characteristic eigenvalues have crossed the imaginary axis, and hence the trivial state has become unstable. Stability is regained in figure 4(c) for $\tau = 7.5$. It can be observed in this picture that there exist different frequencies of oscillations. When τ is larger still, stability is lost again (figure 4(d), $\tau = 11$).

As the system recovers its stability as shown in figure 5(a), one can clearly see the appearance of *beats*. Even though the eigenvalues of the characteristic equation still have negative real part (as can be seen in the way the oscillations decay), it now takes a much longer time for the system to eventually settle onto the trivial equilibrium. Figures 5(b) and 5(d) bear a close resemblance to earlier pictures illustrating the dynamics of the substructure in the unstable regime. Figure 5(c) indicates the beats increase in their amplitude while the decay slows down.

It is interesting to see the behaviour when the curves in figure 3 cross each other. These points correspond to the case when relation (3.8) holds. For $\zeta = 0.05$, the first point p_1 can be found at $(p_1, \tau_1) \approx (0.4453, 7.1859)$. As expected, the system undergoes a codimension-two Hopf bifurcation and exhibits quasi-periodic oscillations as shown in figure 5(a). Finally, figure 5(b) shows the dependence of the Hopf frequency on the delay time τ. At the points of discontinuity, there are two frequencies of oscillations.

Next, the case when the external force is present ($k \neq 0$) will be studied. In figure 7 we show the solution $z(t)$ together with its Fourier spectrum for delay time $\tau = 1.55$, amplitude of perturbation $k = 0.01$, $p = 0.75166$. For this value of p the stability switch occurs at $\tau_c \approx 1.604$ with the corresponding frequency $\varpi_+ = 2$. We have taken perturbation frequency $\Omega = 2.1$ to be close to this frequency in order to study possible resonance. For the above-mentioned parameter values, condition (4.7) holds. One can observe that after some transient period, the solution settles

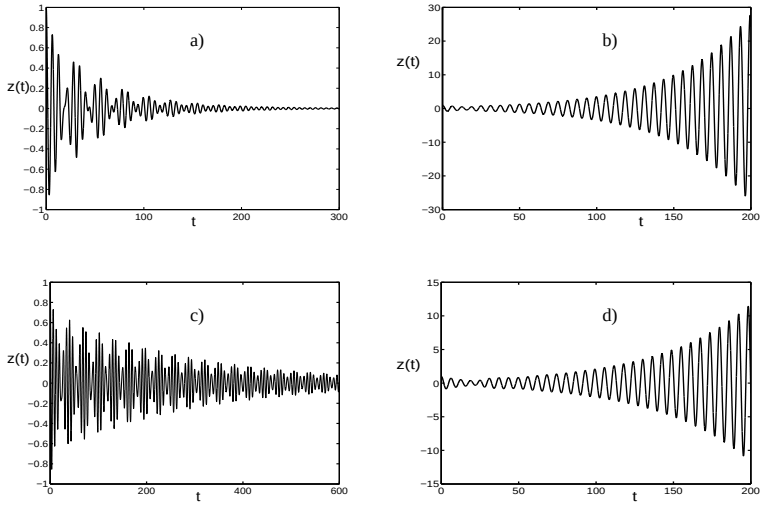

Figure 5. Temporal dynamics of system (3.2) for (a) $\tau = 14$, (b) $\tau = 17$, (c) $\tau = 20$ and (d) $\tau = 23$.

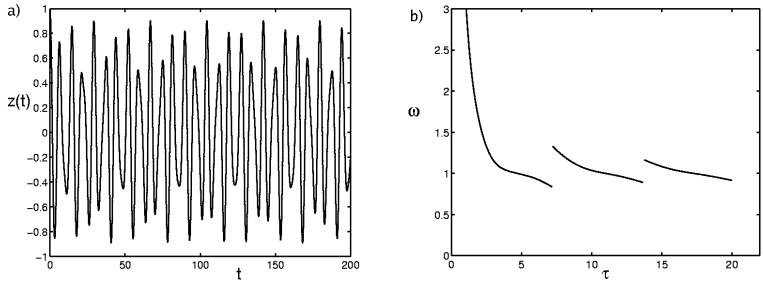

Figure 6. (a) Solution $z(t)$ at the codimension-two point $(p_1, \tau_1) \approx (0.4453, 7.1859)$. (b) Hopf frequency as a function of delay time τ.

onto a stable limit cycle. The Fourier spectrum shown in figure 7 clearly possesses a sharp peak confirming periodic behaviour of the solution. The numerical value of the corresponding oscillation frequency, as found from the Fourier spectrum is $\omega \approx 2.05$. This value lies within 3% of the perturbation frequency $\Omega = 2.1$.

In the previous case the value of the time delay was chosen to lie inside the region of asymptotic stability. In order to illustrate the unstable behaviour of the periodic orbit, we take the delay time $\tau = 1.608$ just outside the stability boundary. For this delay time, condition (4.7) is violated, and the periodic solution, even though it exists, is unstable. The other parameter values are as in figure 7. The temporal dynamics of the solution $z(t)$ is plotted in figure 8 together with the Fourier spectrum. From both pictures one can observe that the periodic solution is modulated on a longer time scale. The Fourier spectrum now contains both the oscillation frequency and a much smaller frequency of the modulation.

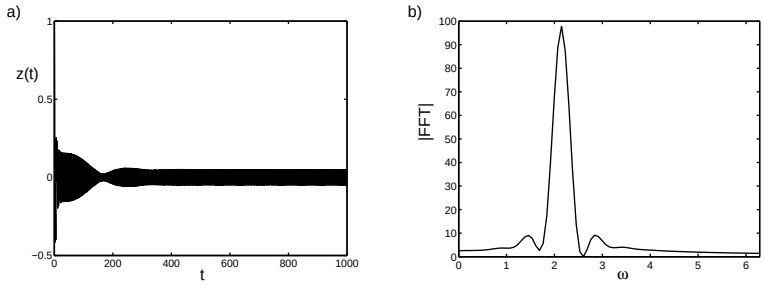

Figure 7. (a) Solution $z(t)$ with $\tau = 1.55$, $k = 0.01$, $\Omega = 2.1$, $p = 0.75166$. (b) Fourier spectrum of the solution.

6. Stability analysis of the full system

Now, we return to system (2.2), and rewrite it (without loss of generality) by omitting the delay in the second equation and setting $F_{\text{ext}} = 0$ to obtain

$$\begin{aligned} & M\ddot{y}(t) + C\dot{y}(t) + Ky(t) + m\ddot{y}(t-\tau) \\ & +m\ell[\ddot{\theta}(t-\tau)\sin\theta(t-\tau) + \dot{\theta}^2(t-\tau)\cos\theta(t-\tau)] = 0, \\ & m\ell^2\ddot{\theta}(t) + k\dot{\theta}(t) + mg\ell\sin\theta(t) + m\ell\ddot{y}(t)\sin\theta(t) = 0. \end{aligned} \tag{6.1}$$

It is more convenient to rewrite these equations as a first order system. In order to do so, we introduce the new variables

$$\mathbf{x} = (x_1, x_2, x_3, x_4)^T = (y, \theta, \dot{y}, \dot{\theta})^T.$$

With these variables, system (6.1) becomes

$$\begin{aligned} \dot{x}_1 &= x_3, \\ \dot{x}_2 &= x_4, \\ \dot{x}_3 &= -\frac{1}{M}\Big[Cx_3 + Kx_1 + m\dot{x}_3(t-\tau) \\ &\quad +m\ell\left[\dot{x}_4(t-\tau)\sin x_2(t-\tau) + x_4^2(t-\tau)\cos x_2(t-\tau)\right]\Big], \\ \dot{x}_4 &= -\frac{k}{m\ell^2}x_4 + \frac{1}{\ell M}\sin x_2\left[Cx_3 - Mg + Kx_1 + \dot{x}_3(t-\tau)\right] \\ &\quad +\frac{m}{M}\sin x_2\left[\dot{x}_4(t-\tau)\sin x_2(t-\tau) + x_4^2(t-\tau)\cos x_2(t-\tau)\right]. \end{aligned} \tag{6.2}$$

The equilibria for this system are $\mathbf{x} = (0,0,0,0)$ and $\mathbf{x_n} = (0, n\pi, 0, 0), n = 1, 2, ...$ Linearization near the trivial steady state $\mathbf{x} = \mathbf{0}$ gives

$$\dot{\mathbf{x}}(t) = A\mathbf{x}(t) + B\dot{\mathbf{x}}(t-\tau),$$

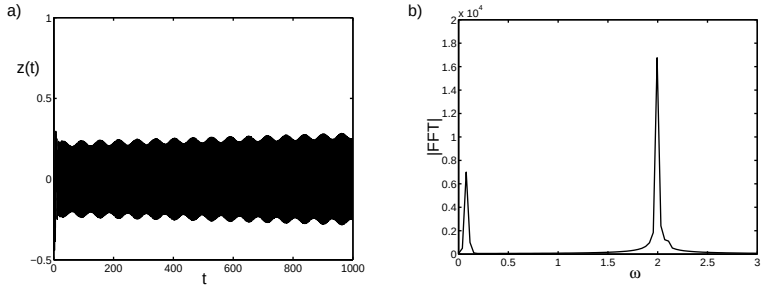

Figure 8. (a) Solution $z(t)$ with $\tau = 1.608$, $k = 0.01$, $\Omega = 2.1$, $p = 0.75166$. (b) Fourier spectrum of the solution.

where matrices A and B are given by

$$A = \begin{pmatrix} 0 & 0 & 1 & 0 \\ 0 & 0 & 0 & 1 \\ -\dfrac{K}{M} & 0 & -\dfrac{C}{M} & 0 \\ 0 & -\dfrac{g}{\ell} & 0 & -\dfrac{k}{m\ell^2} \end{pmatrix}, \; B = \begin{pmatrix} 0 & 0 & 0 & 0 \\ 0 & 0 & 0 & 0 \\ 0 & 0 & -\dfrac{m}{M} & 0 \\ 0 & 0 & 0 & 0 \end{pmatrix}.$$

The characteristic polynomial becomes

$$\left(\lambda^2 + \lambda\frac{k}{m\ell^2} + \frac{g}{\ell}\right)\left(\lambda^2 M + \lambda C + K + \lambda^2 e^{-\lambda\tau} m\right) = 0. \tag{6.3}$$

It is clear that stability is determined by the roots of the second multiplier in equation (6.3).

Similarly, for the steady state $\mathbf{x_n} = (0, n\pi, 0, 0)$ the matrices A and B are given by

$$A = \begin{pmatrix} 0 & 0 & 1 & 0 \\ 0 & 0 & 0 & 1 \\ -\dfrac{K}{M} & 0 & -\dfrac{C}{M} & 0 \\ 0 & (-1)^{n+1}\dfrac{g}{\ell} & 0 & -\dfrac{k}{m\ell^2} \end{pmatrix}, \; B = \begin{pmatrix} 0 & 0 & 0 & 0 \\ 0 & 0 & 0 & 0 \\ 0 & 0 & -\dfrac{m}{M} & 0 \\ 0 & 0 & 0 & 0 \end{pmatrix}.$$

The corresponding characteristic polynomial is now

$$\left(\lambda^2 + \lambda\frac{k}{m\ell^2} + (-1)^n\frac{g}{\ell}\right)\left(\lambda^2 M + \lambda C + K + \lambda^2 e^{-\lambda\tau} m\right) = 0. \tag{6.4}$$

One can now observe that for n odd, which correspond to an upright position of the pendulum, there are always eigenvalues with positive real part. This implies that

Table 1. *Substructure and pendulum parameters*

M[kg]	C[kg/s]	K[N/m]	m[kg]
4	20	5000	0.9

such steady states are always unstable for any value of delay τ, including $\tau = 0$. For the case of n even, the roots are determined by the same equation as in the case $n = 0$ considered above. The second bracket in equations (6.3) and (6.4) is exactly equation (3.3) divided by M in its dimensional form.

7. Experimental results

In the previous sections we studied the stability of the model using analytical and numerical tools. In order to confirm our findings we need to perform some experimental tests, using the real time dynamic substructuring technique. As discussed in the Introduction, the pendulum is the physical substructure, the MSD is modelled numerically in the computer. The numerical model is used to calculate the displacement at the interface due to some external excitation. The displacement is applied to the substructure (pendulum) in real-time using an electro-mechanical actuator (the transfer system). The force acting on the physical substructure is measured via a load cell and fed back to the numerical model. This feedback force is used to calculate the displacement at the interface for the next time step. This process is repeated until the end of the test. To implement real-time tasks a dSpace DS1104 RD Controller Board is used; MATLAB/Simulink is employed to build the numerical model. The dSpace module ControlDesk is used for online analysis and control. The transfer system is an electrically driven ball-screw actuator with an in-line mounted synchronous servo-motor controlled by a servo-drive which applies a displacement to the pendulum pivot point in the vertical direction. The values of the system parameters are given in Table 1. It is worth noting that, since the MSD is represented by a numerical model, M, K and C can be changed easily from one test to another to observe different situations.

The first issue to be addressed in order to be able to develop successful substructuring tests is to ensure numerical model stability. We define stable as bounded input bounded output (BIBO) stable. In this case the output (displacement) will remain bounded for all time, for any initial condition and input. The numerical model in this case is always BIBO stable.

During the experiment the instability due to delay appears as a new frequency in the numerical model displacement, when the stability boundary is crossed. We start with a delay of $0.018s$ (the natural delay time of the transfer system) and the delay will be increased by $0.001s$ increments until the system becomes unstable, and the new frequency appears. The delay time is increased by holding the signals going to the actuator.

Figure 9(a) shows the theoretical stability boundary in the original non-rescaled system (3.1) with the parameters from the Table 1. It also shows the values of the stability switches. Figure 9(b) illustrates the way in which we will explore the stability switches experimentally. In particular, we fix the value of $p = 0.225$ as determined by the parameters, and start simulations in the stable region for a

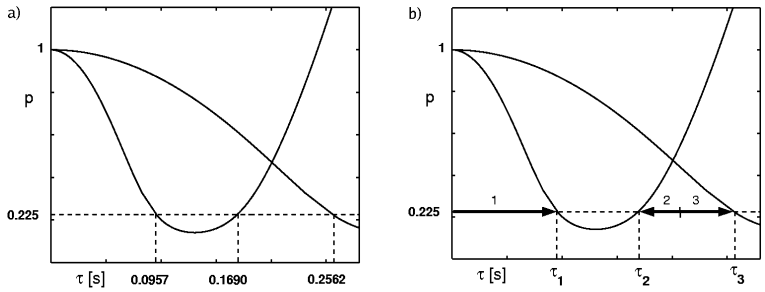

Figure 9. Stability charts showing the stability boundary with the parameters from Table 1: (a) theoretical chart and (b) experimental paths.

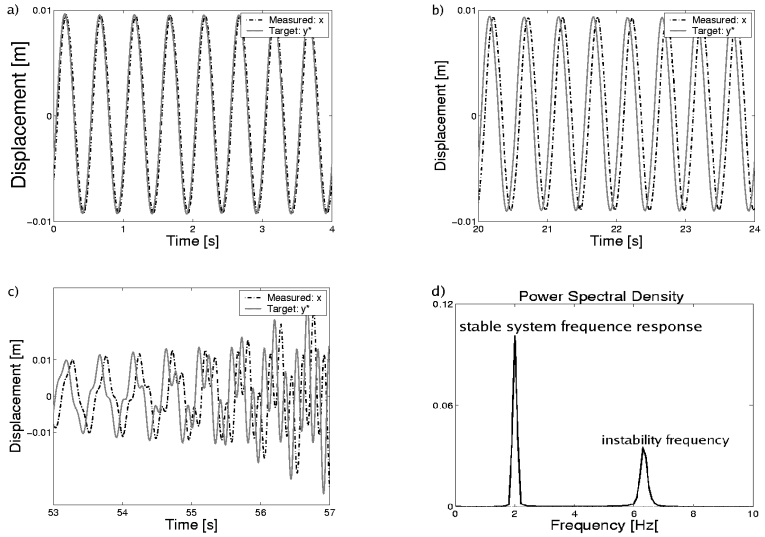

Figure 10. Changes in stability of the system while following path 1 shown in figure 9(b). Numerical model is stable: (a) $\tau = 0.018s$, (b) $\tau = 0.075s$. (c) Instability frequency appears, $\tau = 0.093s$. (d) Fourier spectrum of the response: instability frequency $6.3Hz$.

very small delay time τ. Then we follow path 1 (figure 9(b))until the stability boundary is reached. Once the boundary is crossed, the response of the system grows exponentially making it impossible to continue experimental testing (the actuator cannot achieve the required displacements). Consequently, it is technically impossible to increase the delay further in order to reach the stability area. In order to find the stability boundaries we start with the value of delay time τ inside the next stability region. Decreasing or increasing the delay time, i.e. following path 2 and path 3 in figure 9(b) until the instability frequency appears. In this way the experimental values of stability switches τ_2 and τ_3 will be found.

Figure 10 shows experimental records while following path 1. In figure 10(a) the measured solution x is plotted against its counterpart y^* as determined by the analytical solution of the equation (3.1). The results show that the numerical model is stable until the delay τ reaches the value of $0.093s$, Figure 10(c). At this point an instability frequency of $\omega = 6.3Hz$ appears, as shown in figure 10(d).

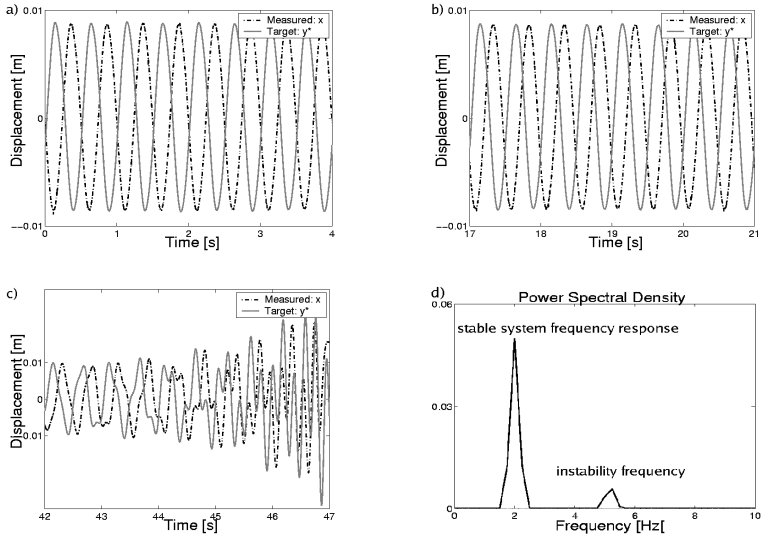

Figure 11. Changes in stability of the system while following path 2 shown in figure 9(b). Numerical model is stable: (a) $\tau = 0.22s$, (b) $\tau = 0.18s$. (c) Instability frequency appears, $\tau = 0.162s$. (d) Fourier spectrum of the response: instability frequency $5.2Hz$.

The experimental eigentriple at the first stability boundary is therefore $(p, \tau, \omega) = (0.225, 0.093, 6.3)$.

Figure 11 illustrates the recorded signals when following path 2, when the delay is decreasing. The numerical model is stable until the delay τ reaches $0.162s$, figure 11(c). The corresponding value of the instability frequency is $\omega = 5.2Hz$, as shown in figure 11(d). Hence, the experimental eigentriple for this crossing of stability boundary is $(p, \tau, \omega) = (0.225, 0.162, 5.2)$.

The experimental results when following path 3 are depicted in figure 12. Now the numerical model remains stable until the delay time τ reaches $0.255s$, and the solution becomes unstable, figure 12(c). In this case, the instability frequency is $\omega = 6.25Hz$, as can be found from the Fourier transform of the solution at this point, as shown in figure 12(d). Therefore, this last boundary point in our analysis is characterized by the experimental eigentriple $(p, \tau, \omega) = (0.225, 0.255, 6.25)$.

Figure 13 shows an excellent agreement between theoretical model and experimental results for stability boundaries. When the stability boundary is crossed, the solution very quickly becomes unstable and develops higher amplitude oscillations and irregular motions. This makes finding experimental values for stability boundary an extremely sensitive problem. This explains slight deviation of experimental values from the analytical prediction as illustrated in figure 13 a). In figure 13 b) we show experimental stability border points corresponding to different values of p.

We summarize analytical and experimental values of the instability frequency in Table 2.

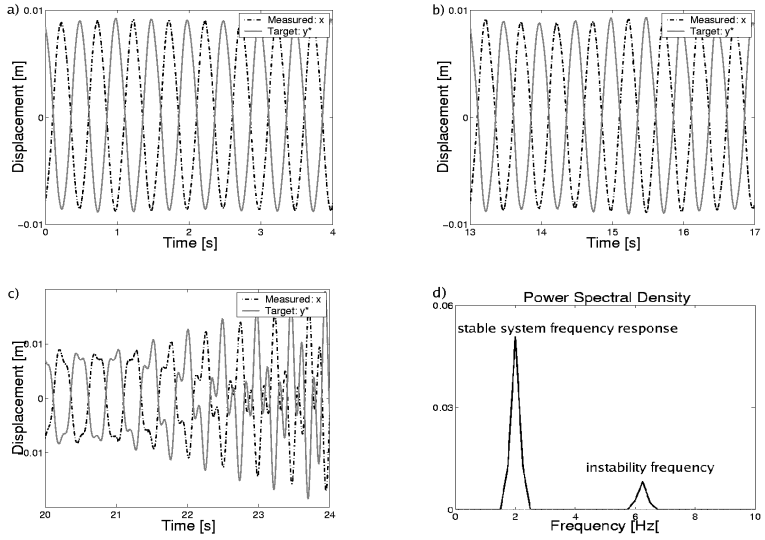

Figure 12. Changes in stability of the system while following path 2 shown in figure 9(b). Numerical model is stable: (a) $\tau = 0.235s$, (b) $\tau = 0.245s$. (c) Instability frequency appears, $\tau = 0.255s$. (d) Fourier spectrum of the response: instability frequency $6.25Hz$.

Table 2. *Theoretical versus experimental instability frequencies, [Hz]*

Instability frequency	ω_a	ω_b	ω_c
Experimental	6.3	5.2	6.25
Theoretical	6.2310	5.2139	6.2310

8. Viscous damping

In this section we consider the effect of velocity feedback on the dynamics of the pendulum-MSD system. This type of feedback becomes important when one takes into account the fact that the pendulum experiences the action of viscous damping. In this case, the vertical equation of motion for the numerical model in the absence of forcing takes the form

$$M\ddot{y} + C_1\dot{y}(t) + Ky(t) + m\ddot{y}(t-\tau) + C_2\dot{y}(t-\tau) = 0, \tag{8.1}$$

where C_1 is the damping of the numerical model, and C_2 is the viscous damping of the pendulum. Using the same scaling as in Section 3 and introducing the new variables

$$\zeta_1 = \frac{C_1}{2\sqrt{MK}},\ \zeta_2 = \frac{C_2}{2\sqrt{MK}},$$

equation (8.1) transforms into

$$\ddot{z} + 2\zeta_1\dot{z} + z + p\ddot{z}(t-\tau) + 2\zeta_2\dot{z}(t-\tau) = 0. \tag{8.2}$$

The characteristic equation is now

$$\lambda^2 + 2\zeta_1\lambda + 1 + p\lambda^2 e^{-\lambda\tau} + 2\zeta_2\lambda e^{-\lambda\tau} = 0. \tag{8.3}$$

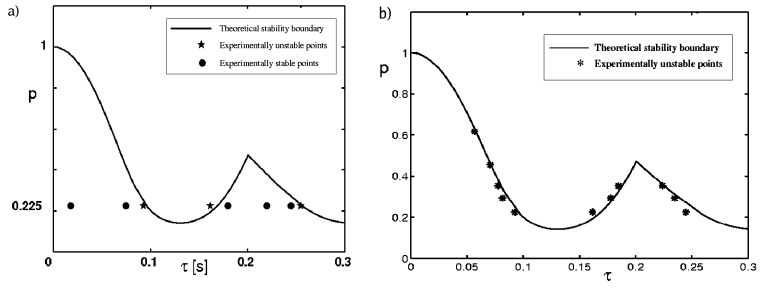

Figure 13. (a) Comparison of experimental results with analytical predictions. (b) Experimental versus theoretical stability border.

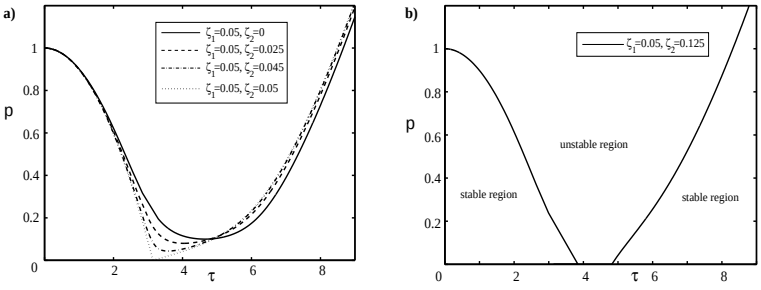

Figure 14. (a) Critical stability boundaries for different values of viscous damping. (b) Disjoint stability boundary for a large value of viscous damping.

Transition to instability occurs when $\lambda = \pm \mathrm{i}\varpi$, $\varpi > 0$. Substituting this into the characteristic equation and separating real and imaginary parts gives the following system

$$\begin{aligned} &-\varpi^2 + 1 - p\varpi^2 \cos \varpi\tau + 2\zeta_2 \varpi \sin \varpi\tau = 0, \\ &2\zeta_1 + p\varpi \sin \varpi\tau + 2\zeta_2 \cos \varpi\tau = 0. \end{aligned} \tag{8.4}$$

Squaring and adding these two equations, we obtain an equation for ϖ, which can be solved to give

$$\varpi_{\pm}^2 = \frac{1}{(1-p^2)} \left[(1 + 2\zeta_2^2 - 2\zeta_1^2) \pm \sqrt{(1 + 2\zeta_2^2 - 2\zeta_1^2) - (1-p^2)} \right]. \tag{8.5}$$

Employing the same methods as the ones used in Section 3, one can prove the following theorem concerning the stability of the trivial solution.

Lemma 8.1. *Let* $1 + 2\zeta_2^2 - 2\zeta_1^2 < 0$. *Then for* $|p| < 1$ *the trivial solution is asymptotically stable for any delay time* $\tau > 0$. *If, however,* $1 + 2\zeta_2^2 - 2\zeta_1^2 > 0$, *then the trivial solution of system (3.2) is locally asymptotically stable in the region*

$$p < 2\sqrt{(1 - \zeta_1^2 - \zeta_2^2)(\zeta_1^2 - \zeta_2^2)}, \tag{8.6}$$

for all positive delay times τ. *In the region*

$$2\sqrt{(1 - \zeta_1^2 - \zeta_2^2)(\zeta_1^2 - \zeta_2^2)} < p < 1,$$

the trivial solution is locally asymptotically stable for values of delay satisfying

$$0 < \quad \tau \quad < \frac{1}{\varpi_+}\left[2\pi - Arccos\,\frac{p(1-\varpi_+^2)-4\zeta_1\zeta_2}{p^2\varpi_+^2+4\zeta_2^2}\right]$$

$$\frac{1}{\varpi_-}\left[2\pi n - Arccos\,\frac{p(1-\varpi_-^2)-4\zeta_1\zeta_2}{p^2\varpi_-^2+4\zeta_2^2}\right] < \tau < \frac{1}{\varpi_+}\left[(2n+2)\pi - Arccos\,\frac{p(1-\varpi_+^2)-4\zeta_1\zeta_2}{p^2\varpi_+^2+4\zeta_2^2}\right],$$

where $n = 1, 2, ...$

It is worth noting that in the limit $\zeta_2 \to 0$ the results of this lemma coincide with those of lemma 3.2. Furthermore, as it is clear from relation (3.7), these stability results are only valid if one imposes an additional but experimentally reasonable requirement $\zeta_2 < \zeta_1$. Physically this means that the viscous damping C_2 of the pendulum is smaller than that of the mass-spring-damper.

We illustrate in figure 14(a) the changes to the stability boundary as the viscous damping is increased from 0 until it reaches the value of the damping of MSD. As the viscosity increases, the stability area gets smaller and stability boundary shifts to the left. Eventually, as can be seen in figure 14(b), after touching zero the stability boundary disintegrates and splits into separate stability regions. As any vibration will eventually die down in these regions, they are called *amplitude death* regions or *death islands* (see, for instance, Xu & Chung 2003). These regions are experimentally important for controlling the stability of the system. Experimental results regarding the stability of the system with viscous damping can be found in Gonzalez-Buelga *et al.* (2005).

We can explain figure 14 physically. The critical stability boundary first touches the τ axis ($p = 0$) when $\zeta_1 = \zeta_2$ and $\tau = \pi$. From equation (8.2) we can see that this corresponds to the case when the contribution to the damping, through the term $2\zeta_1\dot{z}$, is exactly balanced by an equal ($\zeta_1 = \zeta_2$) and opposite (out of phase, since $\tau = \pi$) contribution, through the term $2\zeta_2\dot{z}(t-\tau)$. In this case $\varpi_\pm = 1$ and the resulting solution is neutrally stable since $\lambda = \pm\mathrm{i}$. As ζ_2 then increases, there is a finite range of τ for $p = 0$ when the delayed damping due to the pendulum exceeds that due to the numerical model. In that range the trivial solution is then unstable.

9. Conclusions

In this paper the real-time dynamic substructuring technique has been investigated for the system consisting of a mass-spring-damper and a pendulum attached to it. We introduced a system of two second order delay differential equations, with one of them being neutral. This approach of modelling allows us to account for the delay which naturally arises during the test.

First, we introduced a model consisting of the equations of motion of the MSD and pendulum, where the motion of the pendulum is affected by the delay caused by the transfer system. The model is a nonlinear system of DDEs and we started our analysis by considering the case of small angles. This results in a neutral delay differential equation for the vertical component of motion. We performed a stability analysis for this equation and found regions of stability and instability as the delay time varies. We established not only the points of stability switching but also showed

that there is a finite number of them for fixed system parameters and proposed a scheme for calculating their number. After the presence of a Hopf bifurcation had been established, the stability of the bifurcating periodic solutions was studied using the method of multiple scales. This has also provided analytical expressions for the amplitude and frequency of the periodic orbit, together with an easily verifiable condition for stability.

The numerical simulations which are presented in Section 5 confirm our theoretical findings, and convergence to the steady state can be observed in the stable regions while blow-up of solutions in finite time is shown in the unstable regions. Moreover, quasi-periodic oscillation of the solution is also illustrated and the existence of the *beats* is detected. The Hopf frequency as a function of the delay time shows the presence of two frequencies of oscillation at the codimension-two Hopf bifurcation points. In the case of non-zero forcing our numerical results illustrate two possibilities: the solutions asymptotically approach a stable limit cycle or they are modulated on a long time scale by a growing harmonic. In Section 6 we return to the original system and study its linearized stability.

In order to confirm the validity of our analytical considerations, we performed a series of experimental tests. The stability boundary of the trivial solution was in good agreement with analytical prediction, as were the instability frequencies. The stability of the solution was explored for different values of the delay time τ, and the appearance of instability frequency detected in each case.

We have also considered the case of viscous damping present in the system. This has its effect on the stability boundary as it distorts and shrinks in size. For very large damping the stability area transforms into disjoint death islands separated by instability regions.

Overall, the study in this paper is a first step of modelling nonlinear and more complex substructures using DDEs. Future plans include the modelling of large scale engineering structures, such as suspension bridge cables, and mechanical systems, including the damper units for helicopter rotors.

The authors would like to acknowledge the support of the EPSRC: YK is supported by EPSRC grant (GR/72020/01), KB is supported by EPSRC grant (GR/S31662/01), AGB is supported by EPSRC grant (GR/S49780) and DJW via an Advanced Research Fellowship. SJH is grateful to Centre de Recerca Matemàtica, Bellaterra, Catalunya for providing facilities to complete part of this project.

References

Blakeborough, A., Williams, M.S., Darby, A.P. & Williams, D.M. 2001 The development of real-time substructure testing. *Phil. Trans. R. Soc.* A **359**, 1869 - 1891.

Bonelli, A. & Bursi, O.S. 2004 Generalized-a methods for seismic structural testing. *Earthq. Eng. Struct. Dyn.* **33**, 1067-1102.

Campbell, S.A. 1997 Resonant codimension two bifurcation in a neutral functional differential equation. *Nonl. Anal. TMA* **30**, 4577-4594.

Coveney, V.A., Hunter, G.D. & Spriggs, J. 2001 Is the behaviour of the leg during oscillation linear? *J. Biomech.* **34**, 827-830.

Darby, A.P., Blakeborough, A. & Williams, M.S. 2001 Improved control algorithm for real-time substructure testing. *Earthq. Eng. Struct. Dyn.* **30**, 431-448.

Darby, A.P., Williams, M.S. & Blakeborough, A. 2002 Stability and Delay Compensation for Real-Time Substructure Testing. *J. Engrg. Mech.* **128**, 1276-1284.

Diekmann, O., van Gils, S., Verduyn Lunel, S.M. & Walther, H.-O. 1995 *Delay Equations: Functional, Complex, and Nonlinear Analysis*, vol. 110, Springer-Verlag, New York.

Gonzalez-Buelga,A., Wagg, D.J. & Neil S.A. 2005 A hybrid numerical-experimental model of a coupled pendulum-mass-spring-damper system. submitted to *Int. J. Nonl. Mech.*.

Horiuchi, T., Konno, T. 2001 A new method for compensating actuator delay in real-time hybrid experiments. *Phil. Trans. R. Soc.* A **359**, 1893 - 1909.

Hu, H.Y. & Wang, Z.H. 2002 *Dynamics of controlled mechanical systems with delayed feedback*. Springer-Verlag, New York.

Kuang, Y. 1993 *Delay differential equations with applications in population dynamics*. Academic Press, San Diego.

Lafortune, M.A. & Lake, M.J. 1995 Human pendulum approach to simulate and quantify locomotor impact loading. *J. Biomech.* **28**, 1111-1114.

Nakashima, M. 2001 Development, potential, and limitations of real-time online (pseudo dynamic) testing. *Phil. Trans. R. Soc.* A **359** , 1851-1867.

Pinto, A.V., Pegon, P., Magonette,G. & Tsionis, G.2004 Pseudo-dynamic testing of bridges using non-linear substructuring. *Earthq. Eng. Struct. Dyn.* **33**, 1125-1146.

Stépan, G. 1989 *Retarded dynamical systems: stability and characteristic functions*. Longman, London.

Tondl, A., Ruijgrok, T., Verhulst, F. & R. Nabergoj 2000 *Autoparametric resonance in mechanical systems*. CUP, Cambridge.

Wallace, M.I., Sieber, J., Neild, S.A., Wagg, D.J. & Krauskopf, B. 2005 Delay differential equation models for real-time dynamic substructuring. Accepted for publication in *Earthq. Eng. Struct. Dyn.*.

Wallace, M.I., Neild, S.A. & Wagg, D.J. 2004 An adaptive polynomial based forward prediction algorithm for multi-actuator real-time dynamic substructuring. Submitted to *Proc. R. Soc. Lond.* A.

Wei, J.J. & Ruan, S. 2002 Stability and global Hopf bifurcation for neutral differential equations. *Acta. Math. Sinica* **45**, 93-104.

Williams, M.S. & Blakeborough, A. 2001 Laboratory testing of structures under dynamic loads: an introductory review. *Phil. Trans. R. Soc.* A **359**, 1651 - 1669.

Wu, J. 1996 *Theory and Applications of Partial Functional Differential Equations*. Springer-Verlag, New York, 1996.

Xu, J. & Chung, K.W. 2003 Effects of time delayed position feedback on a van der Pol-Duffing oscillator. *Phys.* D **180**, 17-39.